Entropic attraction and fluid-glass transition in micellar solutions of associative diblock copolymers

Julien Grandjean and Ahmed Mourchid*
Complex Fluids Laboratory, Unité Mixte de Recherche, CNRS-Rhodia (UMR 166), Cranbury, New Jersey 08512, USA
(Received 25 April 2005; published 13 October 2005)

We report quantitative determination of the strength of attraction between spherical micelles of associative diblock copolymers. We offer detailed characterization of the dilute micellar solutions by neutron and dynamic light scattering techniques and by viscometry, and we interpret the data with the aid of the adhesive hard-sphere model. This model permits estimate of the stickiness parameter for varying fraction of stickers on the micelles. At this range of attraction the solutions exhibit, in the crowded regime, rheological and dynamics behavior representative of both repulsive caging and attractive bonding glassy dynamics.

DOI: 10.1103/PhysRevE.72.041503 PACS number(s): 64.70.Pf, 82.70.−y, 83.80.Uv

INTRODUCTION

Colloidal suspensions of monodisperse particles undergo a liquid-crystal phase transition driven solely by a single variable, the volume fraction ϕ [1]. Quenching the crowded suspension from a disordered configuration prevents this entropically-driven phase transition. The operation leads to a liquid-glass phase transition at a volume fraction ϕ_g slightly higher than the volume fraction of crystallization [1–3]. Crowding in suspensions of less monodisperse particles does not induce crystal phases but triggers a glassy state above ϕ_g [4].

One characteristic of the glass phase is the structural arrest of the particles, with the appearance of a nonzero value of the nonergodic parameter, that measures the dynamics of the particles at very long time scales [2]. The glassy phase in model colloids has been the subject of intense investigation both theoretically and experimentally. Most studied systems consisted of colloidal hard spheres where the particles interact through the hard-core repulsive potential, which is the basic model of simple liquids. Particle dynamics is the primary physical concept in the description of the glass transition. The theoretical account for the dynamics was successfully gained from mode coupling theory (MCT) which depicts the evolution of structural arrest in the dynamic structure factor as a function of the control parameter ϕ [5–7]. Several experimental studies have addressed these properties at the onset of the fluid-glass transition [3,4,8]. Light scattering experiments have been successful in exploring the static and the dynamic structure factor over a wide range of length and time scales.

However, many dispersions of colloidal particles encountered in nature or obtained from industrial processes have complicated composition and, consequently, the interactions between the colloids are more complex than the hard-sphere repulsive potential. Therefore, significant differences occur in the state diagram and in the transport properties of particles in the dispersion in contrast with the behavior of simple liquids [9–12]. One basic model that has been extensively used in recent years to account for this complexity is the adhesive hard-sphere model as defined by Baxter [13]. In this model, the hard-core potential is improved by adding a short-ranged attractive square well to the abrupt repulsion. Although the adhesive hard-sphere model is highly idealized, it gives a consistent understanding of some aspects of the colloidal state diagram such as the coexistence of a wide equilibrium fluid-crystal region [11]. Besides these characteristics, the theoretical state diagram exhibits a reentrant fluid-repulsive glass transition at high ϕ and weak attraction and a new class of attractive glass phase where the arrest is realized by increasing both the volume fraction and the attraction [14–17]. At the intersection of the reentrant branch and fluid-attractive glass branch, the dynamics follows a subtle logarithmic decay [18,19], while the mean square displacement evolves as a power law with time [20]. Remarkably, this specific dynamics does not depend on the detailed attractive potential computed as long as the attraction is short ranged compared to the size of the colloids [14,19]. In parallel, these predictions have been confirmed experimentally for very dissimilar systems [21–27], even though the volume fraction threshold value estimated by MCT is lower than the experimental result. On the other hand, the theory estimation of the strength of attraction needed to induce the reentrance is weak, 1 kT or less, for a square well width of few percent of the particles diameter. Experimental determination of phase boundaries has shown that MCT underestimates this parameter [21,28]. To date, entire mapping of the experimental state diagram of attractive colloids in real systems is still lacking. This is primarily due to the complexity of some colloids studied, where the variation of one experimental parameter affects both the volume fraction and strength of attraction [22,23,28].

The above description raises interesting questions on the onset of fluid-glass transition, specifically, at the junction of the three phases. Our goal is to quantitatively determine the strength of attraction in the vicinity of A_3 singularity where the structural arrest is due to both repulsive caging and attractive bonding of the particles [25]. For this purpose, we carry out measurements of the structure of micellar solutions

*Present address: Matière et Systèmes Complexes, Unité Mixte de Recherche, CNRS-Université Paris VII (UMR 7057), 2 Place Jussieu, cc 7056, 75251 Paris Cedex 05, France.

and of the stickiness parameter of dispersions of attractive soft spheres in the dilute regime. We achieve this physically through the use of aqueous micellar solutions of diblock copolymers with a polystyrene (PS) frozen core surrounded by poly(acrylic acid) corona (PAA). The hydrophilic arms carry hydrophobic ethyl acrylate (EA) groups. Bridging between these groups gives rise to an entropic attraction and hereby the stickiness between micelles. We have already shown that these suspensions undergo a reentrant transition in the crowded regime when adhesion is induced between the micelles [25]. Increasing the stickiness further, the dynamics of the suspensions displays a logarithmic decay of the correlation function, which is consistent with MCT findings and the existence of a high order cusplike bifurcation point in the state diagram. In the present study, we use small angle neutron scattering experiments (SANS) to ensure that the addition of hydrophobic units in the corona does not alter the shape of the micelles, and to evaluate their dimension and aggregation number. Low shear viscosity and diffusion coefficient determination for dilute micellar solutions are intended to measure the size of the micelles and the strength of attraction. Consequently, we utilize the adhesive sphere model to interpret the behavior of attractive colloidal suspensions at the onset of the dynamic arrest.

MATERIALS AND METHODS

The diblock polymer is synthesized as polystyrene-poly(ethyl acrylate), PS-PEA, with a molecular weight of 2000–19 468 g/mol, and is obtained as an aqueous suspension of latex particles at approximately 40 wt. % [25,29]. A post-polymerization hydrolysis reaction is performed by adding dropwise 2 M NaOH solution to 10 wt. % polymer solution at a temperature of 90 °C. The hydrolysis reaction converts poly(ethyl acrylate) of the second block to poly(acrylic acid). The amount of NaOH added is dependent on the desired extent of hydrolysis reaction h. The mixture is then held at 90 °C for 24 h. When the hydrolysis is concluded, the copolymer is dialyzed using regenerated cellulose membranes with a molecular weight cutoff of 6000–8000 g/mol (SpectraPor), against deionized water for one week and against water at $p\mathrm{H}=10$ for another week, first to remove impurities and then to normalize the charge density along the polymer backbone. The final product is polystyrene-poly(acrylic acid sodium salt, ethyl acrylate), PS-P(AA/EA). An extent of hydrolysis $h<1$ means that hydrophobic ethyl acrylate units remain in the PAA block and act as stickers between the micelles in H_2O. The fraction of these stickers, $f=1-h$, is the ratio of EA to EA and AA monomers in the second block, and is determined using 400 MHz ^{1}H NMR spectroscopy. For the three systems presented, NMR yields a degree of hydrolysis h of 0.66 ± 0.05, 0.85 ± 0.02 and 0.98 ± 0.02, corresponding to the fraction of stickers $f=0.34$, 0.15, and almost 0, and to total polymer molecular weight $M_w=20.7$, 20.5, and 20.3 kg/mol, respectively. Samples for neutron scattering are prepared by dissolving freeze-dried copolymer in D_2O at the desired concentration and stirring for several days at 80 °C. Stock solutions, at weight concentration $C\approx1$ wt. %, are prepared either by dissolving freeze-dried polymer in H_2O and stirring at 80 °C, or by osmotic stress method by equilibrating copolymer solutions in dialysis membranes with a reservoir of dextran 110 000 aqueous solution at $p\mathrm{H}=10$ for 4 weeks. Diluted samples for viscometry and dynamic light scattering (DLS) are prepared by adding H_2O at $p\mathrm{H}=10$ to the stock solutions at the desired concentration. Diluted samples are filtered through 0.22 μm Millipore filters, sealed and stored prior to the measurements. We check by UV absorption of styrene that filtration does not alter the concentration within experimental uncertainty.

The suspensions in D_2O for SANS ($0.8\leqslant C\leqslant32$ wt. %) are studied at NIST Center for Neutron Research located at NIST in Gaithersburg, MD, on NG3 beamline, with an incident wavelength of 6 Å, and 2 sample to the two-dimensional (2D)-detector distances: 13.1 and 1.33 m, covering scattering vectors q from 0.0035 to 0.3 Å^{-1}. The spectra are collected at room temperature for samples in quartz cells with a path length of 1 and 2 mm, depending on the concentration. D_2O is used to quantify the solvent scattering, and is subtracted off from the data. The spectra, which are also corrected for incoherent scattering estimated from the signal at high q, are subsequently obtained in absolute scale (in [cm^{-1}]).

The scattered intensity per unit volume, $I(q)$ (in [cm^{-1}]), of a monodisperse system can be expressed as the product of the contrast factor, form factor, and structure factor. The contrast factor is dependent on the number density of scatters N (in [cm^{-3}]), on their volume V (in [cm^3]) and on the difference of their scattering length density with the solvent, $\Delta\rho$ (in [cm^{-2}]). The form factor $F(q)$, is characteristic of the shape and the size of the scatters, and the structure factor, $S(q)$, describes correlations between scatters. Within this definition, the scattered intensity is expressed as

$$I(q)=NV^2(\Delta\rho)^2F(q)S(q). \tag{1}$$

We utilize the polydisperse spherical form factor to model scattering intensity of diluted pure PS-PAA copolymer solutions ($f\approx0$) to account for the width of the sphere size distribution assuming a Gaussian size distribution. It is given by [30]:

$$F(q)=\int_0^\infty \frac{9}{\sqrt{2\pi}\sigma}e^{-(r-R_{\mathrm{PS}})^2/2\sigma^2}\frac{[\sin(qr)-qr\cos(qr)]^2}{(qr)^6}dr. \tag{2}$$

This two-parameter model includes R_{PS}, the average PS sphere radius, and σ, the standard deviation of the sphere size distribution. We interpret R_{PS} and σ being characteristic of the PS core size distribution only because the majority of the scattered intensity arises from the contrast between PS and D_2O. The ratio of PS contrast to poly(acrylic acid sodium salt) contrast is 5.35 to 1 (Table I). With this interpretation of form factor, the micelle aggregation number N_{agg} is calculated as

$$N_{\mathrm{agg}}=\frac{4\pi R_{\mathrm{PS}}^3}{3V_{\mathrm{PS}}} \tag{3}$$

where V_{PS} is the volume of the polystyrene block.

TABLE I. Scattering length densities (SLD).

Solute	Scattering length (10^{-12} cm)	Molar volume (cm^3/mol)	SLD ρ (10^{10} cm^{-2})	Contrast in D_2O $(\Delta\rho)^2$ (10^{20} cm^{-4})
D_2O	1.915	18	6.407	0
Styrene	2.33	99	1.417	24.90
PA^-Na^+	2.40	34	4.251	4.65
Ethyl acrylate	1.49	108	0.831	31.09

Because the partially hydrolyzed copolymers are multicomponent systems, the scattered intensity is due to each scatter present in the solution, evenly to ethyl acrylate whose scattering contrast in D_2O is larger than the PS one (Table I). Therefore, the presence of EA monomers in the corona complicate SANS analysis of the form factor for the partially hydrolyzed copolymers. To circumvent this complexity we study the dilution law by examining the evolution of the position of the correlation peaks in concentrated solutions as a function of the PS volume fraction and fraction of stickers. This self-consistent test on the accuracy of the interparticle separation and particle size gives an indication of the variation of the PS sphere radius from dilution equation at different hydrolysis rates, and thus, the aggregation number. The swelling relation is given by [31]

$$\frac{d}{2R_{\mathrm{PS}}} = \alpha\left(\frac{\phi_M}{\phi_{\mathrm{PS}}}\right)^{1/3}, \tag{4}$$

where α and ϕ_M are a constant close to unity and the close packing volume fraction, respectively. The value of these two parameters depends on the structure considered. R_{PS} is the radius of the scattering PS core and ϕ_{PS} is its volume fraction calculated from weight concentration, C, using PS and D_2O densities: 1.05 and 1.10 g/cm^3, respectively. The correlation distance d is extracted from scattering experiments and is related to the position of the correlation peak, $q_0 = 2\pi/d$.

Viscometry is performed using thermostated Couette geometry at 21 °C on a highly sensitive low shear rheometer (Contraves) studying polymer solutions with $0 \leqslant C \leqslant 0.07$ wt. %. Reduced viscosities are obtained by dividing each sample viscosity by the measured viscosity of the solvent (NaOH solution at pH=10). DLS measurements are carried out at 21° C using light scattering setup with an argon laser at a wavelength of 5145 Å, a goniometer (Brookhaven), and a correlator (BI9000AT) for samples in the concentration range $0 \leqslant C \leqslant 0.04$ wt. %. The normalized autocorrelation function is fit to a standard second order cumulant expression, and the quality factor is taken as a measure for the single exponential behavior of the correlation function [32]. We check that the first cumulant is a quadratic function of the wave vector for the most concentrated samples. Then the normalized intensity autocorrelation function is collected for each sample at a scattering angle of 90°. Five to ten runs are performed for each sample studied by viscometry and DLS to ensure reproducibility.

The low-density theory of colloidal suspensions of adhesive hard spheres is well documented [33–36]. The second virial coefficient A_2 is a simple function of the micelle radius, R_h, and stickiness parameter, $1/\tau$, i.e.,

$$A_2 = \frac{4\pi {R_h}^3}{3}\left(4 - \frac{1}{\tau}\right), \tag{5}$$

$$\frac{1}{\tau} = \frac{6\Delta}{R_h}\left[\exp\left(-\frac{U_{\mathrm{min}}}{kT}\right) - 1\right] \tag{6}$$

where Δ and U_{min} are the width and the depth of the attractive square well, respectively. The simplicity of the model leads to quantitative and straightforward determination of the evolution of the low shear viscosity, η, to second order in volume fraction, and of diffusion coefficient D to first order in volume fraction, when accounting for hydrodynamic interactions and assuming that the hard-sphere radius and the hydrodynamic radius are equal [33]:

$$\frac{\eta}{\mu} = 1 + 2.5\phi + \left(6 + \frac{1.9}{\tau}\right)\phi^2, \tag{7}$$

$$\frac{D}{D_0} = 1 + \left(1.45 - \frac{1.12}{\tau}\right)\phi, \tag{8}$$

where μ and D_0 are the solvent viscosity and the bare single particle diffusion coefficient, respectively. Converting the reduced viscosity above to its variation with concentration C, leads to Huggins equation

$$\frac{\eta - \mu}{\mu C} = [\eta]\{1 + k_h[\eta]C\} = [\eta]\left\{1 + \left(0.96 + \frac{0.304}{\tau}\right)[\eta]C\right\}, \tag{9}$$

where $[\eta]$ is the intrinsic viscosity and k_h is the Huggins coefficient. The ratio $[\eta]/2.5 = \phi/C$ is the hydrodynamic volume of the micelles per unit mass [37]. It follows that

$$[\eta] = \frac{10\pi R_h^3 N_a}{3 M_w N_{\mathrm{agg}}}, \tag{10}$$

where Na is Avogadro's number and M_w is the molecular weight of the copolymer. Extrapolation of the Huggins equation to zero concentration gives $[\eta]$, and thus R_h by using N_{agg} measured from SANS data. The slope of this equation yields $1/\tau$.

Similarly, by introducing the intrinsic viscosity in the expression of D we get

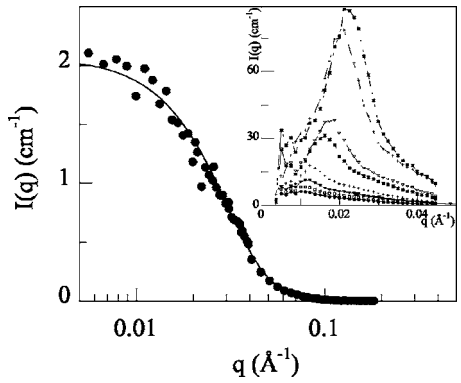

FIG. 1. Scattering intensity $I(q)$ on a sample at $C=0.8$ wt.% and $f=0$. The solid line is a fit to the form factor for polydisperse spheres with a mean radius of 69 Å and polydispersity of 19%. Calculated $I(q)$ is normalized by 1.24 to fit experimental data in absolute scale. Inset: $I(q)$ for concentrated solutions at $f=0$ and $C=2$, 2.5, 3.2, 4.9, 9.65, 14.15, 23.6, and 32 wt.% from bottom to top.

$$\frac{D}{D_0} = 1 + k_d[\eta]C = 1 + \left(0.58 - \frac{0.448}{\tau}\right)[\eta]C \qquad (11)$$

where k_d is the interaction coefficient. Equating D at infinite dilution to the Stokes-Einstein diffusion coefficient D_0 gives R_h and consequently $[\eta]$, whereas the slope of D versus C yields $1/\tau$.

RESULTS AND DISCUSSION

The scattered intensity for a sample at $C=0.8$ wt.% and hydrolysis rate of 100% (fraction of stickers $f=0$) is shown in Fig. 1. For this dilute solution, we do not observe any structure peak for $I(q)$ in the q range investigated. Moreover, the asymptotic evolution in the high q domain shows that $I(q)$ decreases as q^{-4}, representing the Porod regime and demonstrating that the copolymer forms micelles with well-defined interface [38]. For PS-PAA micelles the bare-core approximation provides a good model to account for SANS data in the dilute regime [39]. Thus, the experimental data are fit to the form factor for polydisperse PS core particles in order to gain insight into the micelle characteristics. The scattered intensity in absolute scale for this dilute solution is estimated as

$$I(q) = NV^2(\Delta\rho)^2F(q) = \frac{C}{M}N_aN_{agg}V_{PS}^2(\Delta\rho)^2F(q), \quad (12)$$

where C is the polymer weight concentration. The polydisperse sphere model provides a better fit to the data than the monodisperse sphere model. The model used fits well the scattered intensity in absolute scale even though it overrates the amplitude by 24%. Although this slight difference with the experimental $I(q)$, the resulting fit validates the approximation we use which neglects the contribution of the PAA corona to $I(q)$. The result in Fig. 1 leads to an estimate for the core radius R_{PS} of 69 Å and a polydispersity of 19% ($\sigma=13$ Å). This moderate polydispersity precludes formation

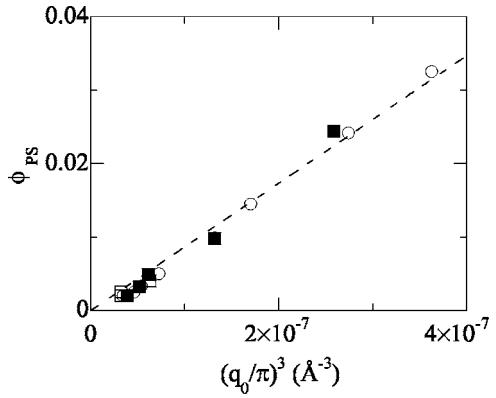

FIG. 2. Dilution law: evolution of the PS volume fraction with correlation peak position for $f=0$ (○), 0.15 (□), and 0.34 (■) with the line representing the linear least-squares fit.

of a colloidal crystal. The data are used to estimate the micelle aggregation number, N_{agg}, given by Eq. (3). With V_{PS}, the volume of the styrene block, calculated as 3164 Å^3, yields $N_{agg}=435$.

In aqueous solutions, all concentrated copolymers form a viscoelastic phase. This phase, associated with a plateau in elastic modulus at low frequency, and the existence of a single correlation peak in the scattered intensity, is identified as a glasslike phase [29]. Furthermore, our scattering data show that the single correlation peak exists in diluted viscous samples and thus the occurrence of the viscous fluid-viscoelastic solid transition is solely induced by structural arrest [25]. The evolution of the scattered intensity with concentration is shown in the inset of Fig. 1 for the fully hydrolyzed copolymer solutions ($f\approx 0$). The position of the peaks, q_0, shifts toward high q values as the micellar concentration increases. In Fig. 2, these results are presented as volume fraction of PS core particles versus $(q_0/\pi)^3$. Investigation of this swelling behavior shows that the micelles follow a three-dimensional dilution law and implies that they are homogeneously distributed in solution since the volume fraction follows a linear decrease to zero with q_0^3. We also observe that the dilution data superimpose for the three fractions of stickers studied, $f=0$, 0.15, and 0.34, meaning that the slope of the linear variation of ϕ_{PS} with $(q_0/\pi)^3$ is independent of the hydrolysis rate. This result strongly suggests that neither the micelle core size R_{PS} nor the intermicellar organization, illustrated by α and ϕ_M values in Eq. (4), are altered by the addition of EA hydrophobes in the corona. It follows that the micellar aggregation number does not vary in the present study.

It is worth adding that the independence of dilution law from f is in agreement with Poon and co-workers findings showing constant peak position for suspensions with weak attraction, i.e., in the reentrant region of the phase diagram [28]. Beyond the reentrant region, these authors observed a slight decrease in correlation distance for constant volume fraction upon increasing the strength of attraction in suspensions of hard spheres, and they concluded that the decrease of correlation length is exclusively due to particle trapping in the attractive well.

The presence of short-ranged and weak attraction between the micelles favors the trapping effect in colloidal suspen-

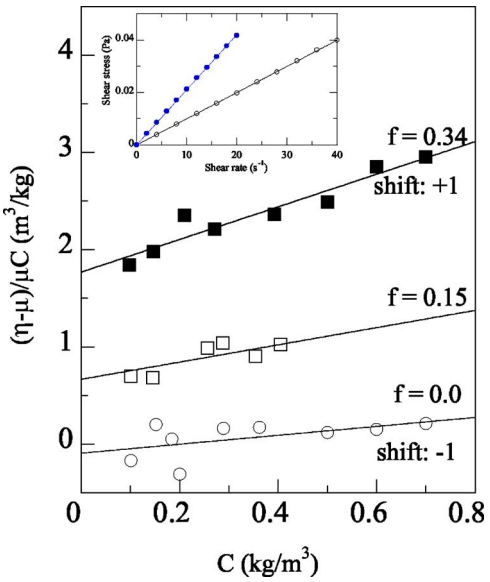

FIG. 3. Variation of reduced viscosities with concentration for $f=0$ (○), 0.15 (□), and 0.34 (■). For clarity, data for $f=0$ and $f=0.34$ are shifted by −1 and +1, respectively. Inset: shear stress versus shear rate for $C=0$ (○) and $C=0.06$ wt. %, $f=0.15$ (●). The lines represent linear least-squares fits.

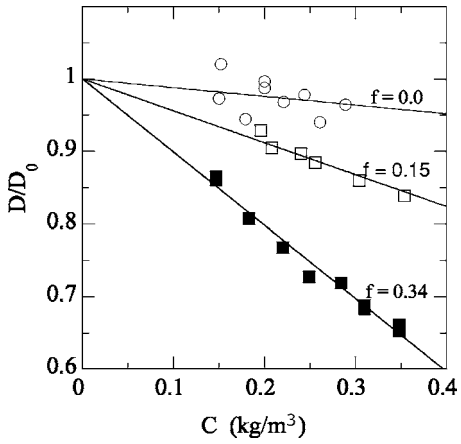

FIG. 4. Variation of diffusion coefficients with concentration for $f=0$ (○), 0.15 (□), and 0.34 (■), normalized by $D_0(10^{-12}\ \mathrm{m^2/s})=2.10$, 2.44, and 2.26 respectively, with lines representing linear least-squares fits.

sions and causes the formation of a colloidal glass at high concentration. Assuming that the hard-sphere radius in the adhesive hard-sphere model corresponds to the hydrodynamic radius R_h in Eqs. (9) and (11), we can determine from the linear variation of transport data (η and D) with C both R_h and $1/\tau$ as well as their variation with f.

The reduced viscosities increase linearly with concentration in the dilute regime as shown in Fig. 3 for the three fractions of stickers: 0, 0.15, and 0.34. Fitting the experimental data to the Huggins equation [Eq. (9)] yields $[\eta]$ and the Huggins coefficients shown in Table II. The intrinsic viscosity shows minor and nonmonotonous fluctuations with the number of stickers on the micelles. It is worth mentioning that the experimental uncertainty on $[\eta]$ computed in Table II does not take into consideration the uncertainty on concentration and could thus explain the fluctuations in $[\eta]$. Thus the nearly constant value of $[\eta]$ for the three systems studied suggests that the micellar hydrodynamic volume per unit mass is almost constant for these systems. By using Nagg =435 obtained from SANS analysis, we deduce the hydrodynamic radius of the micelles, reported in Table II. From the slope of data in Fig. 3, we clearly observe that the extracted value for the Huggins coefficients k_h for the fully hydrolyzed copolymer ($f\approx 0$), characterizing pair interactions and shown in Table II, is consistent with what we could expect for a polymer in a good solvent [33]. As f increases, k_h increases and corresponds to increasing attraction between the micelles.

The isolated micelle diffusion coefficient, obtained by extrapolating the mutual diffusion coefficient data shown in Fig. 4 to zero concentration shows nearly constant D_0 value for the three fractions of stickers (Table III). By using Nagg=435, we deduce the corresponding intrinsic viscosity for these three systems. Remarkably, DLS results are in good agreement with viscometry results. The curves in Fig. 4 show linear variation of D with C, with a negative slope for the three systems. The value of k_d, describing pair interactions, is slightly negative for $f\approx 0$ (Table III) and becomes increasingly negative as f increases, signing the presence of larger attractive interactions. Although, the data from light scattering exhibit a slight negative contribution to k_d at zero fraction of stickers rather than the positive and well-defined excluded volume contribution of 0.58 [Eq. (11)], these measurements show clearly the effect of increasing the number of ethyl acrylate hydrophobes in the corona on inducing large entropic attraction between these micelles in aqueous solution.

HYDRODYNAMIC RADIUS

The SANS study shows that varying the hydrolysis rate between 66% and 100% does not alter the shape and the size of the micellar core. These micelles act as frozen structures

TABLE II. Viscometry data ($N_{agg}=435$).

f	M_w (kg/mol)	$[\eta]$ (m^3/kg)	R_H (Å)	k_h	l/τ
0	20.3	0.9±0.1	1080±40	0.80±0.40	−0.5±1.3
0.15	20.5	0.6±0.1	947±53	2.00±0.50	3.4±1.7
0.34	20.7	0.77±0.09	1032±40	2.90±0.35	6.4±1.2

TABLE III. DLS data (N_{agg}=435).

f	D_0 (10^{-12} m^2/s)	R_H (Å)	$[\eta]$ (m^3/kg)	$-k_d$	$1/\tau$
0	2.10±0.20	1025±100	0.77±0.22	0.16±0.16	1.7±0.4
0.15	2.44±0.04	883±15	0.49±0.03	0.91±0.10	3.3±0.3
0.34	2.26±0.03	953±13	0.61±0.03	1.65±0.20	5.0±0.5

and they do not re-organize upon dilution in water or addition of stickers in the hydrophilic corona up to f=0.34. It results that the aggregation number remains constant. The determination of the intrinsic viscosity for each system studied shows that this is an unvarying parameter within acceptable experimental uncertainty. Since the aggregation number does not change for f between 0 and 0.34, it results that the hydrodynamic radius obtained from viscometry is constant for these PS-P(AA/EA) micelles, in agreement with DLS data for R_h. We also know that the micelle brushes are completely stretched for pure PS-PAA spherical micelles [40]. Thus, insertion of up to 34% of hydrophobic monomers in the polyelectrolyte block does not alter the full extension of the coronal layer. Our micelle characteristics are consistent, to some extent, with those of Groenewegen *et al.* [40] who demonstrated that neither the PS core radius nor the stretching of the PAA corona are affected when the degree of ionization of the poly(acrylic acid) block is changed between 50% and 100% for PS-PAA micelles.

The agreement of viscometry results with those from DLS might seem disputable, primarily because viscometry method is less powerful than DLS. On the one hand, viscometry data are deduced from a higher order variation of viscosity with concentration [Eq. (9)], as disclosed in a larger experimental uncertainty. On the other hand, and as against DLS, the shear experiment is a perturbative method that forces relative motion of the micelles [33,37]. However, in our case, the ratio of applied shear rate ($\dot{\gamma}$ between 1 and 20 s^{-1}) to diffusion coefficient ($\sim 2\times 10^{-12}$ m^2/s) leads to very low Peclet number, $\mathrm{Pe}=R_h^2\dot{\gamma}/D_0$ between 0.005 and 0.1, meaning that viscometry measurement does not significantly drive the microstructure out of equilibrium.

So far the effect of polydispersity on the size of the micelles and how their static radius is connected to their hydrodynamic radius were not considered. Polydispersity is believed to increase the difference between these two radii [41]. However our previous results show that when using the hydrodynamic radius to scale the volume fraction at the onset of fluid-glass transition, this value was estimated to 0.64, slightly larger than the value expected for a monodisperse system [29]. Therefore, despite the systematic uncertainty in the estimation of the hard-sphere radius, polydipsersity seems to have a minor effect in our system.

STICKINESS PARAMETER

To characterize our systems, we envision the micelles to interact via an adhesive hard-sphere potential. By using the relationship between the interaction coefficients in reduced viscosity and in mutual diffusion coefficient and the stickiness parameter $1/\tau$ [Eqs. (9) and (11)], we obtain the values of $1/\tau$ reported in Tables II and III.

Both measurements show that the entropic attraction increases with the fraction of stickers present in the corona, with $1/\tau$ going from almost 0 for $f\approx 0$ to $1/\tau$=6 for f =0.34. For $f\approx 0$, there is almost no ethyl acrylate sticker in the corona. Therefore, the micelles should act as nearly hard spheres due to the repulsive potential created by the dense PAA brushes which form a steric barrier. DLS measurements return a slightly finite value for the stickiness parameter. Several assumptions we use could be incorrect. First, the hard-sphere repulsion model is undoubtfully less appropriate for the soft micelles we are dealing with, albeit the large aggregation number that should produce an abrupt excluded volume repulsion. Second, we use the hydrodynamic radius to calculate the second virial coefficient, rather than the excluded volume radius of the micelles which should be smaller than R_h [32]. If these assumptions are at fault, the method could yield far overestimated second virial coefficient since it is highly dependent on the volume of micelles. To be entirely accurate, the data analysis should have consisted in measuring excluded volume and hydrodynamic contributions to D and η in the repulsive system ($f\approx 0$), and then subtracting off these contributions when attraction is added on the micelles (f=0.15 and 0.34). Accounting for this reduces $1/\tau$ measured from DLS by 1.7 but it also increases the discrepancy with viscometry data. Overall, our determination of the stickiness parameter is in good agreement with visual observation of phase behavior of these aqueous copolymer solutions that never show gas-liquid phase separation up to f=0.5, and strongly suggests that for f between 0 and 0.34 $1/\tau$ should lie far below the critical point located at $1/\tau_c$=10.2 (and ϕ_c=0.12) [33].

Given the value of the stickiness parameter above, it is tempting to evaluate the two parameters of the attractive square well used to model the data. Since we envision it is the contact between hydrophobic monomers on two separate micelles that provides the stickiness, we might assume that the range of attraction is equal to the size of two EA monomers at contact which yields $\Delta/R\approx 0.005$, a very small value that brings this system close to the sticky hard-sphere model. However it is likely that the attraction ranges over a length scale larger than the size of two monomers, particularly for the highest value of f, where we anticipate hydrophobic monomers to be likely nearest neighbors along the micellar arms. Our previous results show that for this micellar copolymer aqueous suspensions, $1/\tau$ of 5–6 for f=0.34 correspond to the region of the state diagram where we observe the logarithmic decay of the correlation function in the con-

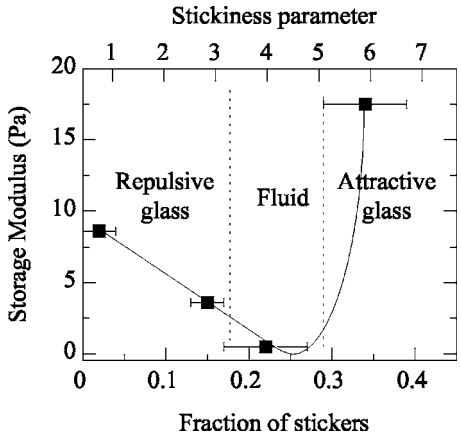

FIG. 5. State diagram deduced from elasticity measurements (Ref. 25) at fixed $C=2.1$ wt. %. Error bars on fraction of stickers are deduced from NMR measurements. The corresponding stickiness parameter is the average of viscometry and DLS data. The solid line is a guide to the eye and vertical dotted lines indicate phase boundaries.

centrated regime [25]. The logarithmic decay is a proposed signature of the A_3 singularity located nearby the reentrant branch end point [15]. The measured $1/\tau$ of 5–6 is consistent with molecular dynamics simulation using Asakawa-Oosawa attractive potential with depletion range of $0.1\times R$ and showing an increase of particle dynamics when $U_{\min}$ increases from 0 up to $2\times kT$ which corresponds to the exploration of the reentrant branch up to its end point [21]. In the adhesive hard-sphere potential [Eq. (6)], these two parameters correspond to a stickiness parameter $1/\tau\sim 4$. Figure 5 summarizes these data and shows phase boundaries obtained by measuring elastic modulus for samples at a fixed polymer concentration, $C=2.1$ wt. %, and varying f [25].

Although our measurements at low volume fraction provide an estimate of the stickiness parameter, they only permit to compare this micellar system with the polymer-colloid mixture to a limited extent. In the latest system, the attractive depletion is well described by the Asakura-Oosawa form and the attraction range, Δ, depends only on polymer size while in our micellar system, the model we use to fit the data does not provide a separate estimate of Δ and $U_{\min}$. The comparison between these two systems is thus restricted to the determination of $1/\tau$ in the domain of the state diagram nearby A_3 singularity. More explicitly, we cannot pursue the analysis further, that is, the weakness of the two methods used is that the contributions of Δ and $U_{\min}$ to $1/\tau$ cannot be separated. Thus, while it is evident that the strength of attraction increases with the addition of more stickers on the micelles, it is not clear at the present stage how the range of attraction is connected to this fraction of stickers.

CONCLUSIONS

In summary, SANS data on dilute copolymer solutions are modeled using spherical form factor for a polydisperse hard-sphere system, where a Gaussian distribution is used to characterize the polydispersity, and the resulting parameters give information on the PS core. Our SANS data on concentrated samples show that the micelle aggregation number, N_{agg}, does not vary as f increases. These results are in agreement with our previous SANS study of the form factor of diluted PS-P(AA/EA) copolymer micellar solutions with a molecular weight of 5300–5800 g/mol and varying f [25]. The similarities between the scattering curves demonstrate that the shape and the size of the micelles are not altered when varying the amount of stickers on the micelles. This result is confirmed for the full size of the micelles, where the viscometry technique on PS-P(AA/EA) solutions of varying f at infinite dilution returns an intrinsic viscosity consistent with the hydrodynamic radius determined from dynamic light scattering.

Although we notice a discrepancy between the expected hard-sphere virial coefficient and the measured value for $f\approx 0$, the approximate adhesive hard-sphere model describes well these micelles and offers an acceptable description of the effects of pair interactions on transport properties. The use of this basic square well model leads to a reasonable account for the results in diluted solutions and provides excellent connection to the general behavior of the phase diagram of attractive colloids, and to their dynamics in the vicinity of the fluid-glass transition.

ACKNOWLEDGMENTS

The authors thank Dr. Gilda Lizzaraga of the Synthesis and Development Laboratory in Cranbury, NJ, for synthesizing the PS-PEA copolymers, and Dr. Steve Kline and Dr. Boualem Hammouda for providing assistance with the SANS experiments at NIST. We acknowledge the support of the National Institute of Standards and Technology, U. S. Department of Commerce, in providing the neutron facilities used in this work. The SANS data are based upon activities supported in part by the National Science Foundation under agreement No. DMR-9986442.

[1] P. N. Pusey and W. van Megen, Nature (London) **320**, 340 (1986).
[2] P. N. Pusey and W. van Megen, Phys. Rev. Lett. **59**, 2083 (1987).
[3] W. van Megen and S. M. Underwood, Phys. Rev. E **49**, 4206 (1994).
[4] E. Bartsch, M. Antonietti, W. Schupp, and H. Sillescu, J. Chem. Phys. **97**, 3950 (1992).
[5] W. Götze and L. Sjögren, Rep. Prog. Phys. **55**, 241 (1992).
[6] C. A. Angell, in *Complex Behavior of Glassy Systems*, edited by M. Rubi and C. Perez-Vincente (Springer, Berlin, 1997).
[7] U. Bengtzelius, W. Götze, and A. Sjölander, J. Phys. C **17**, 5915 (1984).
[8] P. N. Segre and P. N. Pusey, Phys. Rev. Lett. **77**, 771 (1996).

[9] W. C. K. Poon, J. S. Selfe, M. B. Robertson, S. M. Ilett, A. D. Pirie, and P. N. Pusey, J. Phys. II **3**, 1075 (1993).
[10] P. N. Segre, V. Prasad, A. B. Schofield, and D. A. Weitz, Phys. Rev. Lett. **86**, 6042 (2001).
[11] S. M. Ilett, A. Orrock, W. C. K. Poon, and P. N. Pusey, Phys. Rev. E **51**, 1344 (1995).
[12] D. Rosenbaum, P. C. Zamora, and C. F. Zukoski, Phys. Rev. Lett. **76**, 150 (1995).
[13] R. J. Baxter, J. Chem. Phys. **49**, 2770 (1968).
[14] J. Bergenholtz and M. Fuchs, Phys. Rev. E **59**, 5706 (1999).
[15] L. Fabbian, W. Götze, F. Sciortino, P. Tartaglia, and F. Thiery, Phys. Rev. E **59**, R1347 (1999); **60**, 2430 (1999).
[16] G. Foffi, K. A. Dawson, S. V. Buldyrev, F. Sciortino, E. Zaccarelli, and P. Tartaglia, Phys. Rev. E **65**, 050802(R) (2002).
[17] E. Zaccarelli, G. Foffi, K. A. Dawson, S. V. Buldyrev, F. Sciortino, and P. Tartaglia, Phys. Rev. E **66**, 041402 (2002).
[18] W. Götze and M. Sperl, Phys. Rev. E **66**, 011405 (2002).
[19] K. Dawson, G. Foffi, M. Fuchs, W. Götze, F. Sciortino, M. Sperl, P. Tartaglia, T. Voigtmann, and E. Zaccarelli, Phys. Rev. E **63**, 011401 (2000).
[20] F. Sciortino, P. Tartaglia, and E. Zaccarelli, Phys. Rev. Lett. **91**, 268301 (2003).
[21] K. N. Pham, A. M. Puertas, J. Bergenholtz, S. U. Egelhaaf, A. Moussaïd, P. N. Pusey, A. B. Schofield, M. E. Cates, M. Fuchs, and W. C. K. Poon, Science **296**, 104 (2002).
[22] T. Eckert and E. Bartsch, Phys. Rev. Lett. **89**, 125701 (2002).
[23] W. R. Chen, S. H. Chen, and F. Mallamace, Phys. Rev. E **66**, 021403 (2002).
[24] D. Pontoni, T. Narayanan, J. M. Petit, G. Grubel, and D. Beysens, Phys. Rev. Lett. **90**, 188301 (2003).
[25] J. Grandjean and A. Mourchid, Europhys. Lett. **65**, 712 (2004); J. Grandjean and A. Mourchid, in *Self-Assembled Nanostructured Materials*, edited by Y. Lu, C. J. Brinker, M. Antonietti, and C. Bai, MRS Symposium Proceedings No. 775 (Materials Research Society, Warrendale, PA, 2003), p. 231.
[26] W. C. K. Poon, MRS Bull. **29**, 96 (2004).
[27] L. Cipelletti and L. Ramos, J. Phys.: Condens. Matter **17**, R253 (2005).
[28] K. N. Pham, S. U. Egelhaaf, P. N. Pusey, and W. C. K. Poon, Phys. Rev. E **69**, 011503 (2004).
[29] S. R. Bhatia and A. Mourchid, Langmuir **18**, 6469 (2002); S. R. Bhatia, M. Crichton, A. Mourchid, R. K. Prud'homme, and J. Lal, Polym. Prepr. (Am. Chem. Soc. Div. Polym. Chem.) **42**, 326 (2001).
[30] J. S. Higgins and H. C. Benoît, *Polymers and Neutron Scattering* (Clarendon Press, Oxford, 1994).
[31] S. T. Hyde, Colloids Surf., A **103**, 227 (1995).
[32] M. M. Kops-Werkhoven and H. M. Fijnaut, J. Chem. Phys. **74**, 1618 (1981).
[33] Q. T. Pham, W. B. Russel, J. C. Thibeault, and W. Lau, Macromolecules **32**, 2996 (1999).
[34] B. Cichocki and B. U. Felderhof, J. Chem. Phys. **93**, 4427 (1990).
[35] P. W. Rouw and C. G. de Kruif, J. Chem. Phys. **88**, 7799 (1988).
[36] J. M. Woutersen, J. Mellema, C. Blom, and C. G. de Kruif, J. Chem. Phys. **101**, 542 (1994).
[37] W. B. Russel, D. A. Saville, and W. R. Schowalter, *Colloidal Dispersions* (Cambridge University Press, Cambridge, England, 1989).
[38] G. Porod, in *Small Angle X-ray Scattering*, edited by O. Glatter and O. Kratky (Academic Press, London, 1982).
[39] C. Svaneborg and J. S. Pedersen, Macromolecules **35**, 1028 (2002).
[40] W. Groenewegen, S. U. Egelhaaf, A. Lapp, and J. R. C. van der Maarel, Macromolecules **33**, 3283 (2000); W. Groenewegen, A. Lapp, S. U. Egelhaaf, and J. R. C. van der Maarel, *ibid.* **33**, 4080 (2000).
[41] P. N. Pusey, in *Liquids, Freezing and the Glass Transition*, edited by J. P. Hansen, D. Levesque, and J. ZinnJustin (North-Holland, Amsterdam, 1991).